Acta Pharmaceutica Sinica B 2015;5(6):554–563

HOSTED BY

ELSEVIER

Chinese Pharmaceutical Association
Institute of Materia Medica, Chinese Academy of Medical Sciences

Acta Pharmaceutica Sinica B

www.elsevier.com/locate/apsb
www.sciencedirect.com

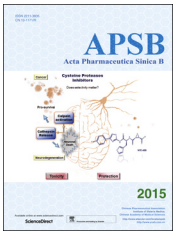

ORIGINAL ARTICLE

The antitumor effect of tanshinone IIA on anti-proliferation and decreasing VEGF/VEGFR2 expression on the human non-small cell lung cancer A549 cell line

Jun Xie[a,†], Jiahui Liu[a,†], Heng Liu[a], Shihui Liang[b], Meigui Lin[c], Yueyu Gu[a], Taoli Liu[a], Dongmei Wang[d], Hui Ge[e,*], Sui-lin Mo[a,*]

[a]*Department of Traditional Chinese Medicine, The First Affiliated Hospital, Sun Yat-sen University, Guangzhou 510080, China*
[b]*Huanghuagang Street Community Health Service Center, Guangzhou 510095, China*
[c]*Liwan District Shiweitang Street Community Health Service Center, Guangzhou 510360, China*
[d]*School of Pharmaceutical Sciences, Sun Yat-sen University, Guangzhou Higher Education Mega Center, Guangzhou 510006, China*
[e]*Health Care and Physical Examination Center, The First Affiliated Hospital, Sun Yat-sen University, Guangzhou 510080, China*

Received 15 June 2015; received in revised form 1 July 2015; accepted 11 July 2015

KEY WORDS

Non-small cell lung cancer;
Tanshinone IIA;
VEGF/VEGFR signal pathway;
Molecular docking

Abstract The effects of tanshinone IIA on the proliferation of the human non-small cell lung cancer cell line A549 and its possible mechanism on the VEGF/VEGFR signal pathway were investigated. The exploration of the interaction between tanshinone IIA and its target proteins provides a feasible platform for studying the anticancer mechanism of active components of herbs. The CCK-8 assay was used to evaluate the proliferative activity of A549 cells treated with tanshinone IIA (2.5 − 80 μmol/L) for 24, 48 and 72 h, respectively. Flow cytometry was used for the detection of cell apoptosis and cell cycle perturbation. VEGF and VEGFR2 expression were studied by Western blotting. The binding mode of tanshinone IIA within the

Abbreviations: ADM, adriamycin; CAM, chorioallantoic membrane; CCK-8, cell counting kit-8; DMSO, dimethylsulfoxide; EPCs, endothelial progenitor cells; FBS, fetal bovine serum; FCM, flow cytometry; HRP, horseradish peroxidase; IC_{50}, 50% inhibitory concentration; MD, molecular dynamics; mOS, median overall survival; NS, normal saline; NSCLC, non-small cell lung cancer; PI, propidium iodide; PKB/AKT, protein kinase B; RMSD, root-mean-square deviation; Tan IIA, tanshinone IIA; tRR, tumor response rate; vdW, van der Waals force; VEGF, vascular endothelial growth factor

*Corresponding authors. Tel./fax: +86 20 87334601.
E-mail addresses: gehui2009gh@126.com (Hui Ge), mosuilin@mail.sysu.edu.cn (Sui-lin Mo).

†These authors made equal contributions to this work.

Peer review under responsibility of Institute of Materia Medica, Chinese Academy of Medical Sciences and Chinese Pharmaceutical Association.

http://dx.doi.org/10.1016/j.apsb.2015.07.008

crystal structure of the VEGFR2 protein was evaluated with molecular docking analysis by use of the CDOCKER algorithm in Discovery Studio 2.1. The CCK-8 results showed that tanshinone IIA can significantly inhibit A549 cell proliferation in a dose- and time-dependent manner. Flow cytometry results showed that the apoptosis rate of tested group was higher than the vehicle control, and tanshinone IIA-treated cells accumulated at the S phase, which was higher than the vehicle control. Furthermore, the expression of VEGF and VEGFR2 was decreased in Western blot. Finally, molecular docking analysis revealed that tanshinone IIA could be stably docked into the kinase domain of VEGFR2 protein with its unique modes to form H-bonds with Cys917 and π–π stacking interactions with Val848. In conclusion, tanshinone IIA may suppress A549 proliferation, induce apoptosis and cell cycle arrest at the S phase. This drug may suppress angiogenesis by targeting the protein kinase domains of VEGF/VEGFR2.

1. Introduction

Lung cancer is the most common malignant tumor. It was estimated that 1.82 million people were diagnosed with lung cancer, and 1.6 million deaths were associated with lung cancer worldwide 2012[1]. The tumor response rate (tRR) of standard platinum based chemotherapy for advanced lung cancer is only 25%–35%, with the median overall survival (mOS) of 8–10 months[2,3].

Adriamycin (ADM), also known as doxorubicin, is a well-known chemotherapeutic drug, the anti-cancer effect of which has been widely affirmed. Based on the effective anti-tumor effects of ADM, it was often chosen as a positive control in experiments. However, the serious side effects and the emergence of drug resistance are becoming the major limitations for its application. Therefore, a search for new anti-tumor drugs which can minimize associated toxicities to non-cancerous tissues is on the forefront of scientific research[4].

Vascular endothelial growth factor (VEGF) promotes vasculogenesis and angiogenesis that enhance blood vessel growth in tissues and maintains blood supply to tissues. Overexpression of VEGF in cancer tissues was found associated with tumor growth and metastasis[5]. Therefore, a drug that is potent regulating expression of VEGF in cancer tissues is attracting more and more attention in the anti-cancer drug development.

Bevacizumab is the first approved recombinant humanized monoclonal antibody that specifically targets VEGF-A in USA[6]. The review of di Costanzo et al.[7] found bevacizumab plus platinum-based chemotherapy significantly increased mOS and tRR compared to platinum-based chemotherapy alone in the treatment of advanced non-small cell lung cancer (NSCLC).

A recent double-blind, multicenter, phase III trial, comprising a total of 276 patients were randomly divided to the group of carboplatin/paclitaxel plus bevacizumab and the group of carboplatin/paclitaxel plus placebo for advanced or recurrent nonsquamous NSCLC. The results showed the bevacizumab group significantly improved the tRR (54% *vs.* 26%, respectively), as well as the mOS (24.3 *vs.* 17.7 months, respectively) compared to the placebo group[8]. Bevacizumab appeared more effective in lung cancer patients who were VEGF-positive[9]. However, the toxicity profiles of this drug mainly include hemorrhage, hypertension, thrombosis and cardiac ischemia[10]. Therefore, a continuous search for new anti-tumor drugs which can minimize associated toxicities to non-cancerous tissues is on the forefront of scientific research.

Salvia miltiorrhiza Bunge is the dry root and rootstock of salvias and known as 'Danshen' in traditional Chinese medicine. In tradition, *S. miltiorrhiza* Bunge has been used for promoting blood circulation, removing blood stasis, clearing away toxic material, relieving restlessness and eliminating edema[11]. Modern pharmacological studies find that the active ingredients of *S. miltiorrhiza* Bunge have pro-cardiovascular effects such as expanding the coronary artery, increasing blood flow in the coronary artery, anti-oxidant, anti-inflection, liver protection, immunity regulation and anti-tumor effect.

Tanshinone IIA (Tan IIA) is one of the main fat-soluble compositions in the root of red-rooted salvia (Fig. 1). The anti-tumor effect of Tan IIA includes inhibiting tumor cell proliferation, disturbing tumor cell cycle, promoting tumor cell apoptosis, and inhibiting tumor cell invasion and transfer[11,12].

In various cancer cell studies, researchers[11–16] found the antitumor effect and anti-angiogenic effect of Tan IIA were associated with inhibiting the expression of VEGF. These studies also showed inhibiting the expression of VEGF did not appear in normal cells.

While there has been a lot of research on the relationship between Tan IIA and the expression of VEGF, whether Tan IIA has an influence on the combination of VEGF and its receptors in lung cancer metastasis remains unclear. Therefore, we proposed that the Tan IIA's antitumor effect may be associated with the regulation of VEGF/VEGFR signal pathway. We conducted the present study to explore the mechanism of Tan IIA-induced inhibition of tumor progression and regulated angiogenesis *via* VEGF/VEGFR signaling pathway in the NSCLC cell line A549.

2. Materials and methods

2.1. Materials

The human non-small cell lung cancer A549 cell line was purchased from the Cell Bank of the Chinese Academy of Sciences (Shanghai, China). Tan IIA (1,6,6-trimethyl-6,7,8,9-tetrahydrophenanthro[1,2–*b*]furan-10,11-dione Danshen ketone, $C_{19}H_{18}O_3$, >97% HPLC) was purchased from Sigma-Aldrich (St. Louis, USA), and prepared as a 10 mmol/L stock solution in dimethylsulfoxide (DMSO, Sigma-Aldrich). The solution was kept in dark and −20 °C, and serially diluted in a RPMI 1640 medium immediately prior to experiments. Adriamycin hydrochloride ($C_{27}H_{29}NO_{11}$, 98.0%–102.0% HPLC) was purchased from Sigma-Aldrich and prepared as a 13.79 mmol/L stock solution in normal saline (NS). The solution was kept in dark and −20 °C and serially diluted in a RPMI 1640 medium immediately prior to experiments. RPMI1640 medium and fetal bovine serum (FBS)

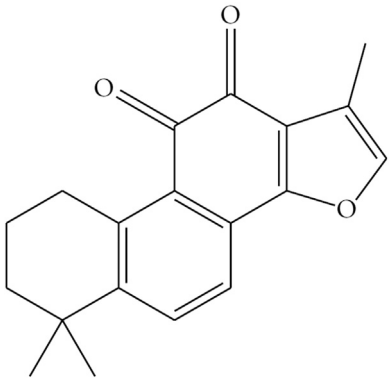

Figure 1 The structure of tanshinone IIA (from PubChem compound).

were purchased from American Hyclone Company (Logan, USA). Pancreatin was supplied by Gibco (Carlsbad, USA). Cell Counting Kit-8 (CCK-8) was purchased from Dojindo Molecular Technologies Inc. (Kumamoto, Japan). The Annexin V-FITC apoptosis detection kit and KeyGEN DNA content quantitation assay (cell cycle) were obtained from KeyGEN BioTECH (Nanjing, China). Rabbit anti-human VEGF monoclonal antibody, rabbit anti-human VEGFR2 monoclonal antibody, rabbit anti-human GAPDH polyclonal antibody and goat anti-rabbit horseradish peroxidase (HRP)-conjugated secondary antibody are obtained from Cell Signaling Technology (Beverly, USA).

2.2. *Cell line and cell culture*

A549 cell line were cultured in RPMI1640 medium, supplemented with 10% FBS in a humidified incubator at 37 °C with 5% CO_2 atmosphere. Cells in logarithmic phase will be used in the experiment.

2.3. *Detection of the anti-proliferative effect of Tan IIA*

A549 cells were counted in logarithmic phase and 6000 cells (90 μL volume) were placed in 96-well plates. 10 μL varying concentrations of Tan IIA (final concentrations 80, 60, 40, 30, 20, 15, 10, 5 and 2.5 μmol/L) and ADM (final concentrations 8, 4, 2, 1, 0.5 and 0.25 μmol/L) were added into drug groups, while negative control group (vehicle group) was only added 10 μL DMSO or normal saline without Tan IIA or ADM. Cells were incubated for an additional 2 h with CCK-8 reagent (100 μL/mL medium) and the absorbance was read at 450 nm using a microplate reader (BioTek, Winooski, 126 VT, USA). Cell proliferation inhibition rates were calculated according to the following formula: the proliferation inhibition ratio $(\%) = 1 - [(A1 - A4)/(A2 - A3)] \times 100$, where, $A1$ is the OD value of drug experimental group, $A2$ is the OD value of blank control group, $A3$ is the OD value of the RPMI1640 medium without cells, and $A4$ is the OD value of drugs with the same concentration as $A1$ but without cells. The IC_{50} (50% inhibitory concentration) value, which represents the concentration of the drug that demonstrates 50% of cell growth inhibition, was calculated by nonlinear regression analysis using GraphPad Prism software (San Diego, USA).

2.4. *Morphological changes of A549 cells*

A549 cells (10^5 cells/mL, 2 mL in 6-well plates) were grown to 70% confluence, and Tan IIA and ADM were added in final concentrations of 31 μmol/L and 2.5 μmol/L (IC_{50} value for 48 h) respectively, along with control and vehicle groups. Morphological changes of A549 cells were observed by optical microscope every 12 h.

2.5. *Cell apoptosis measurements by flow cytometry (FCM)*

Designated cells (10^5 cells/mL, 2 mL/well) were allowed to adhere and yield 80% confluence. Cells were then treated with 31 μmol/L Tan IIA for 48 h. To exclude the impact of the DMSO solution, we added an equal volume of DMSO in the vehicle group, and an equal volume of RPMI1640 medium in the blank control group. Cells were collected by centrifugation and washed twice with ice-cold PBS. The collected cells were then resuspended in 200 μL of binding buffer and incubated with 5 μL each of Annexin V-FITC and propidium iodide (PI) for 15 min in the dark, at room temperature, per the manufacturer's instructions. The cells were analyzed immediately after staining, using a FACScan flow cytometer (Becton-Dickinson). For each measurement, at least 20,000 cells were counted. Each experiment was repeated 3 times.

2.6. *Cell cycle studies using flow cytometry*

Cells were counted in logarithmic phase (10^5 cells/mL, 2 mL in 6-well plates), which were synchronized by medium exposure, with a low concentration of FBS for 24 h for the induction of cell cycle arrest. The culture medium was then replaced with a nutrient-rich medium, and the cells in Tan IIA group were treated with 31 μmol/L Tan IIA for 48 h. The grouping methods and drug treatments were the same as above. Cells were then harvested, washed twice with cold PBS and fixed with 75% cold ethanol at 4 °C for 24 h. Cells were then incubated with RNase A (50 μg/mL) at 37 °C for 30 min then labeled with propidium iodide (PI, 0.1 mg/mL) followed by incubation at room temperature in the dark for 30 min prior to analysis. For each measurement, at least 20,000 cells were counted. Fluorescence intensity of the stained cells was measured using flow cytometry (Beckman Coulter, USA). Data were analyzed using ModFit (Verity Software House, Inc., Topsham, USA). These experiments were repeated 3 times.

2.7. *VEGF and VEGFR2 protein expression with Western blot*

A549 cells treated with Tan IIA (31 μmol/L) and ADM (2.5 μmol/L) for 48 h were collected, along with blank and vehicle groups. Cells were rinsed twice with PBS and lysed in ice-cold lysis buffer for 30 min with occasional rocking. The lysates were clarified by centrifuging them at 12,000 rpm, for 5 min at 4 °C. The protein concentration of each supernatant was determined using the BCA kit (Cwbiotech , Beijing, China). Analysis was performed with 8% SDS-PAGE separation gel and 60 μg proteins were transferred to PVDF membrane. The membrane was blocked using blocking buffer for 2 h at room temperature, and incubated overnight at 4 °C with specific primary antibodies (VEGF, 1:1000; VEGFR2, 1:500; GAPDH, 1:2000). Subsequently, the membrane was washed three times with TBST buffer and incubated with horseradish peroxidase (HRP)-conjugated secondary antibodies (1:1000) for 1 h at room temperature, and washed extensively before detection. The membranes were subsequently developed using enhanced chemiluminescence reagent (Millipore, Billerica, USA) and exposed to film according to the manufacturer's protocol. GAPDH was used as the internal reference. Relative optical density (ROD, ratio to GAPDH) of each blot band was quantified by using National Institutes of Health (NIH) image software (Image J 1.36b).

2.8. Molecular docking

To predict the potential interaction of Tan IIA and the VEGFR2 protein, the CDOCKER module in Discovery Studio (DS) 2.1 (Accelrys Software Inc., San Diego, USA) was applied to our molecular docking algorithm. The three dimensional (3D) crystal structure of VEGFR2 was selected from PDB (http://www.rcsb.org/pdb/) with an ID of 3VHE. The 3D structure of Tan IIA was downloaded from The PubChemProject (http://www.pubchem.ncbi.nlm.nih.gov/) with a CID of 164676. The DS2.1 was run using a localhost9943 server.

VEGFR2 and Tan IIA docking procedure includes the following steps. First, preparation for Tan IIA and VEGFR2: the water molecules in the protein were removed and the hydrogen atoms were added to the receptor protein. VEGFR2 and Tan IIA were refined with CHARMm respectively. Secondly , the active site of VEGFR2 was defined by two methods: one is according to internal ligand's binding site, the other is defined automatically with DS 2.1, and then selected by relevant references. Thirdly, Tan IIA was docked into the active site of 3O96 with proper parameter setting and a series of algorithm.

Specific docking procedures were as follows by CDOCKER: the grid origin was located at the center of the active site of VEGFR2 with a minimum of 21.0Å or the largest ligand dimension +5.0Å as the side length. A grid spacing of 0.5Å was used. For each defined van der Waals force (vdW) or electrostatic probe, the interactions with all protein atoms were stored at these grid points. For ligand atoms located between grid points, a tri-linear interpolation was used to approximate the energies. A harmonic potential with the force constant of 300 kcal/mol was applied outside the grid boundary. Starting from the Tan IIA of input configuration, 10 different orientations were randomly generated by translating the center of the ligand to the grid within the receptor active site, and performing a series of random rotations, and then docked into the protein (3O96), *i.e.*, moved into the center of the grid. Each orientation was subjected to simulated annealing molecular dynamics simulation. A molecular dynamics (MD) simulation was run consisting of a heating phase from 300 to 700 K with 2000 steps, followed by a cooling phase back to 300 K with 5000 steps. The energy threshold for vdW was set at 300 K. We further refined the simulation result by running a short energy minimization, consisting of 50 steps of steepest descent followed by up to 200 steps of conjugate gradient using an energy tolerance of 0.001 kcal/mol.

2.9. Statistical analysis

Statistical analyses were performed with mean ± standard deviation (SD) values using Student's *t*-test and two-way analysis of variance (ANOVA) with the Bonferroni's correction. Statistical significance was concluded at $P<0.05$.

3. Results

3.1. Anti-proliferative effects on cells

Both Tan IIA and ADM had anti-proliferative effects on A549 cells. The effects were dose- and time-dependent, with more pronounced effects being observed following higher concentrations and after longer exposure times. At the same time, the effect of ADM was more obvious than that of Tan IIA: the IC_{50} of ADM after 24, 48 and 72 h were 14.36, 2.34 and 0.99 μmol/L, respectively. In contrast, IC_{50} values for Tan IIA were 145.3, 30.95 and 11.49 μmol/L, respectively (Fig. 2A and B).

3.2. Effects of Tan IIA and ADM on A549 morphology

Obvious apoptosis and cell growth inhibition of A549 cells were observed after drug treatment for 48 h (concentrations used were approximately IC_{50} values: Tan IIA 31 μmol/L or ADM 2.5 μmol/L on A549). The morphology changes included blebbing, loss of cell membrane asymmetry, attachment and cell shrinkage (Fig. 3).

3.3. Effects of Tan IIA on apoptosis

Drug-induced apoptosis was tested with the Annexin V/PI double dye kit. Annexin V can combine with cytomembrane in early stage of apoptosis while PI can enter cells in the middle or advanced stage of apoptosis and combine with the cell nucleus. FCM analyses yielded cell histograms consisting of four quadrants (Fig. 4). The dots in the upper left quadrant represent the injured cells during the process of collecting cells. The dots in the lower left quadrant represent normal cells. The dots in the upper right quadrant represent apoptotic cells in advanced stage and necrotic cells. And the dots in the lower right quadrant represent apoptotic cells in early stage. Thus, the ratio of apoptotic cells in each group should be the sum of the ratio of the upper right and lower right quadrants. As a result, the ratios of apoptotic cells in blank control group, vehicle control group and Tan IIA group respectively were: 11.27%, 11.12% and 22.22%. The laboratory findings revealed: only a small part of cells go to apoptosis in the blank control group and the results exhibited no significant differences between the blank control group and vehicle group, indicating good condition of the cells. After a 48 h treatment with Tan IIA (31 μmol/L), the ratio of cell apoptosis in the Tan IIA group increased ($P<0.001$ *vs.* the vehicle group, Fig. 4).

3.4. Effects of Tan IIA on cell cycle

Cell cycle experiments were performed with the DNA quantitation assay. The results found that following 48 h of exposure, the cell cycle distribution of blank group and vehicle groups exhibited no significant difference, demonstrating that DMSO at very low concentrations had no obvious effect. In A549 cells, after 48 h of exposure to Tan IIA (31 μmol/L), the ratio of cells in G1 stage and G2 stage decreased while the ratio in S stage increased *vs.* vehicle. However, none of these changes achieved statistical significance except the S phase arrest ($P<0.05$), indicating that Tan IIA may have inhibiting effect on A549 cells in S stage (Fig. 5).

3.5. Effect of Tan IIA on VEGF/VEGFR2 protein expression

Western blotting found that 48 h exposures to Tan IIA (31 μmol/L) or ADM (2.5 μmol/L) in A549 cells, downregulated expression of VEGF and VEGFR2 protein in both drug treatment groups *vs.* vehicle (Fig. 6). Protein expression was not changed significantly in the blank and vehicle groups.

3.6. Virtual docking technique simulates the approach of the interaction between Tan IIA and VEGFR2

Docking calculations *via* the CDOCKER docking module in DS2.1 can accurately simulate the docking of small molecules to the active

sites of macromolecules. After docking with endogenous ligand by CDOCKER, the root-mean-square deviation (RMSD) is medially about 0.35Å. While the RMSD, after docking again with endogenous ligand by LigandFit, is medially about 0.91Å, which indicates the root-mean-square of the ligand calculated by CDOCKER module has less displacement as compared to the endogenous ligand in single crystal diffraction diagram. Thus, the docking results calculated by CDOCKER module are more accurate, supporting our choice of CDOCKER for the present work.

Using the protein crystal structure of VEGFR2 and its binding site in the PDB database permitted a resolution of the 3VHE three-dimensional structure at 1.55Å (Fig. 7A). This structure, consisting of 359 amino acid residues and a peptide chain, contains the protein kinase structural domain of VEGFR2. In this structural domain, there is a new inhibitor that belongs to pyrrole pyrimidines. In addition to the endogenous ligand binding site, automatic searching of DS2.1. revealed 7 active sites. Characterization of site1 (Fig. 7B) shows a large overlap with the endogenous ligand-binding region. Integration of these results with related articles confirms the binding site of the endogenous ligand as the binding site being presently explored. The center of a region reachable by an appropriate small molecule would include the amino acid residues, whose radius is less than 5Å are: Leu840, Glt841, Val848, Ala866, Val867, Lys868, Glu885, Ile888, Leu889, Ile892, Val898, Val899, Val914, Val916, Gle917, Phe918, Cys919, Lys920, Phe921, Gly922, Asn923, Leu1019, Cys1024, Ile1025, His1026, Leu1035, Ile1044, Cys1045, Asp1046 and Phe1047.

Simulations of the approach of Tan IIA and its protein binding site revealed 10 configurations (Fig. 7C). Tan IIA can dock stably with the kinase structural domain of the endogenous ligand binding

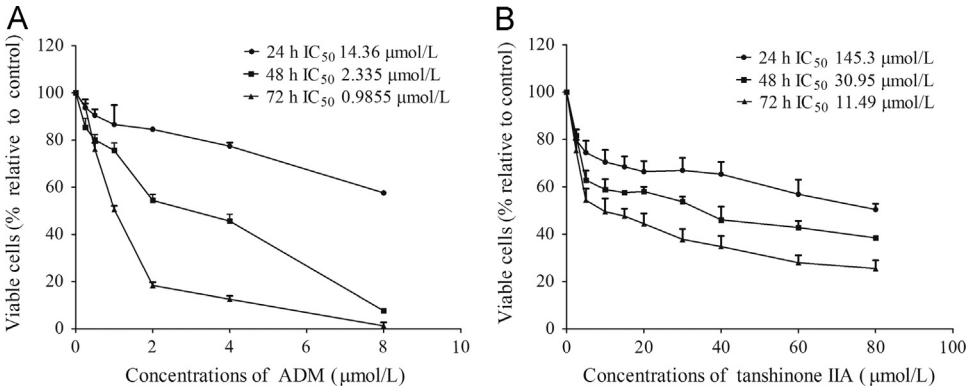

Figure 2 Inhibitive effects of adriamycin and tanshinone IIA respectively on A549 cells. Cells were treated with different concentrations of adriamycin (A) and tanshinone IIA (B) for 24, 48 and 72 h, then assayed by CCK8 method. Data were derived from three independent experiments.

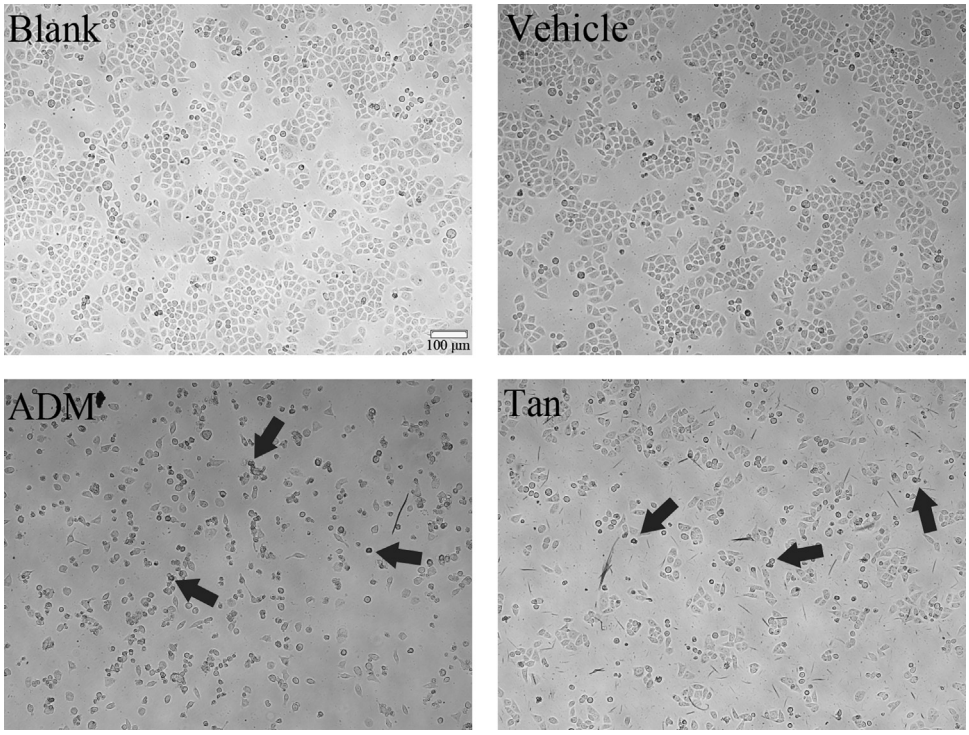

Figure 3 Effect of tanshinone IIA and adriamycin on morphology of A549 cells. A549 cells were treated with tanshinone IIA (31 μmol/L) or adriamycin (2.5 μmol/L) for 48 h and then observed under optical microscope.

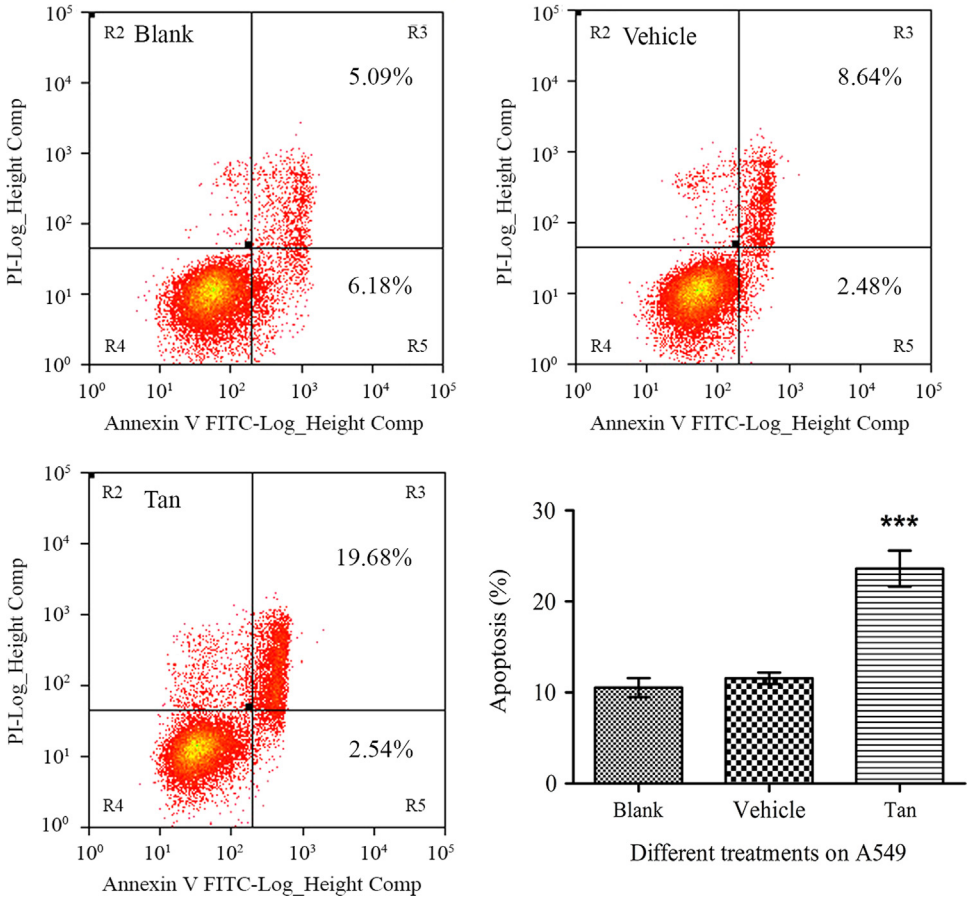

Figure 4 Effect of tanshinone IIA on apoptosis of A549 cells. The apoptotic status was determined with Annexin V/PI staining method. Representative FCM profiles of cells were shown by a cytometric analysis. The drug-treated cells showed significantly increased apoptosis. $^{***}P<0.001$ *vs.* vehicle.

site (Fig. 7C). In this kinase structural domain, the two amino acid residues, Val848 and Cys917, are related to the interaction between Tan IIA and VEGFR2. All of the 10 configurations of Tan IIA can form hydrogen bond with Cys917 and in the meantime the 10 poses can form π–π interaction with Val848 (Fig. 7D).

4. Discussion

In this study, ADM was used as a positive control to ensure the accuracy of the methods and experimental design. In addition, equivalent volumes of DMSO were used in the negative control groups. As explained earlier, the CCK8 method was used to investigate A549 cell proliferation, and the FCM used to explore cell apoptosis and cycle changes. The findings indicate that Tan IIA and ADM have remarkable inhibitory effects on A549 cell proliferation which are in a dose- and time-dependent manner. Most importantly, Tan IIA at a concentration of 31 μmol/L can induce apoptosis and S phase arrest.

Our finding of Tan IIA-induced A549 cells' apoptosis is consistent with other studies[12,17–19]. Tung's research[16] found that, the proteins involved in the S to M phase transition were suppressed by Tan I or Tan II treatment (1, 5, 10 and 25 μmol/L Tan I for 24 h) in human lung adenocarcinoma cell lines (A549, CL1-0 and CL1-5), indicating that Tan I and Tan II are likely to slow the progression of cells through the S and G2 phases of the cell cycle. Wei et al.[20] found that when the renal cancer cell line 786-O cells were treated with Tan IIA (0, 2, 4 and 8 μg/mL) for 24 h, the percentage of cells in the S phase was 10.0%, 11.5%, 20.4% and 23.3%, indicating that Tan IIA treatment induces S phase arrest in 786-O cells.

There are disagreements across laboratories over effects of these drugs on the cell cycle. Ma and others[21] hold the view that Tan IIA causes G0/G1-phase cell-cycle arrest in the NSCLC cell line H1299 cells. These experiments showed that treatment of H1299 cells with Tan IIA (4 μmol/L) for 48 h, the proportion of cells at the G0/G1 phase increased more than 10% as compared with the control.

Based on these findings, we propose that different doses of Tan IIA on different cells may result in different cell cycle effects at different post-treatment times. We propose that low doses of Tan IIA may contribute to cell cycle arrest at the G1 phase after short treatment time, whereas higher doses of Tan IIA may lead to S phase blockade after longer exposure time. However, there is not enough published data to support a powerful conclusion on the cell cycle effects caused by Tan IIA.

In recent decades, scientists have found that VEGF can stimulate vascular endothelial cell division and proliferation, inhibit cell apoptosis, increase vascular permeability, and promote revascularization and angiogenesis in different tissues. Cell-dependent VEGF signaling relies on the specific membrane receptors Flt-1, VEGFR2 and VEGFR3. VEGF activates the tyrosine kinase after combining with the receptors outside cells, and then promotes receptor phosphorylation and the ensuing signal transduction mechanisms. The overall impact of VEGF in endothelial cells is controlled by combinations with Flt-1 and VEGFR2. VEGF B exerts its function *via* Flt-1 while VEGF C and VEGF D exert their function *via* VEGFR2 and VEGFR3. sFlt-1 and sVEGFR2 have strong antagonistic effects

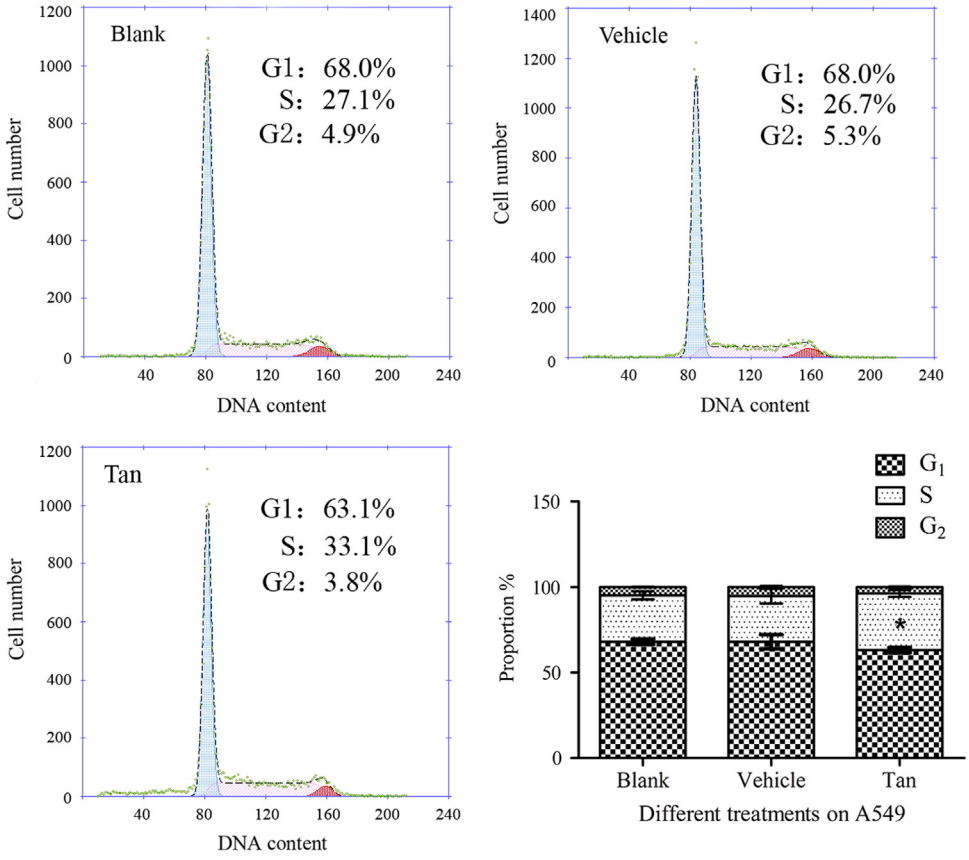

Figure 5 Effect of tanshinone IIA on cell cycle of A549 cells. Representative FCM profiles of cells were shown by a cytometric analysis. The drug-treated cells showed small difference in S phase. $^{*}P<0.05$ *vs.* vehicle.

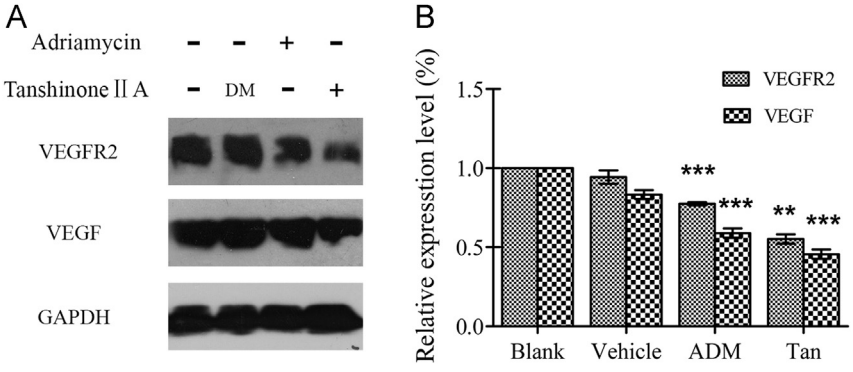

Figure 6 Effect of tanshinone IIA and adriamycin respectively on VEGF and VEGFR2 expression of A549 cells. Western-blot assay showed that the drug-treated A549 cells had significantly difference on the expression level of VEGF and VEGFR2, compared to vehicle group. $^{***}P<0.001$, $^{**}P<0.01$ *vs.* vehicle.

against VEGF. These soluble receptors can combine with VEGF and interdict its biological activity, destroying the integrity and permeability of vascular walls, thereby attenuating angiogenesis. VEGF has strong affinity for both Flt-1 and VEGFR2. The activity of Flt-1 tyrosine kinase is only one tenth of that of VEGFR2. This receptor can exert strong biological effects after stimulation[22]. It is known that VEGFR2 controls the signal transduction of VEGF.

Since the present results found that the expression of VEGF and VEGFR2 in A549 cells declined after treatment of Tan IIA (31 μmol/L) after 48 h, we suggest that the mechanism of Tan IIA induction of A549 cell apoptosis might be associated with Tan IIA's inhibition of VEGF and VEGFR2 expression, thereby interdicting the combination of VEGF and VEGFR2, and blocking the VEGF/VEGFR signal pathway. Such effects would inhibit the generation of new vessels of tumor cells.

This hypothesis is consistent with the results of other researchers studying the anti-tumor cell effect of Tan IIA. Their findings showed that Tan IIA can inhibit cell proliferation, angiogenesis, migration and tube formation of human umbilical vascular endothelial cells. Techniques used included chorioallantoic membrane (CAM), rat

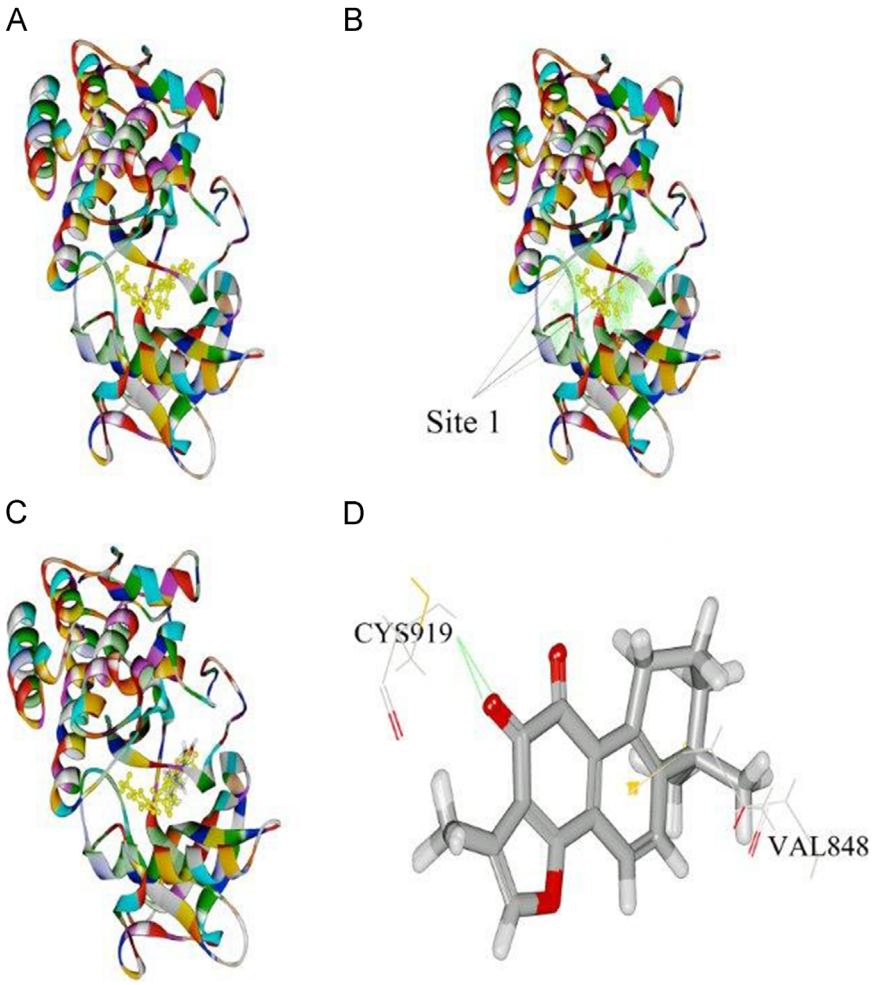

Figure 7 Interaction of tanshinone IIA and VEGFR-2 protein. (A) The 3D structure of crystal structure of human VEGFR-2 (3VHE) with a kinase domain Inhibitor. The solid ribbon is the 3D structure of crystal structure of 3VHE with a 1.55Å resolution. In the center of 3VHE is a kinase domain inhibitor bound in the interface. (B) The binding site1 of 3VHE through auto-searching of DS2.1 (green). (C) The 10 poses from tanshinone IIA were docked into the endogenous ligand's active site of VEGFR-2. (D) Ten random poses of tanshinone IIA binding to the endogenous ligand's active site of 3VHE presented at least 2 residues involved in the interactions potentially: H-bonds with Cys917, aromatic interactions with Val848.

aortic ring assays and Western blotting. Xing et al.[15] reached the conclusion that Tan IIA may inhibit endothelial cell function *via* the simultaneous inhibition of the VEGF/VEGFR2 signaling pathway and regulation of MMP-2/-9 production.

Tung et al.[16] found that both Tan I and Tan II can attenuate lung tumorgenesis *via* inhibition of VEGF, cyclin A and cyclin B expressions in A549, CL1-0 and CL1-5 cell lines. The authors concluded that blockade of the tumor-activated cell cycle pathway may be a critical mechanism for the observed antitumorigenic effects of Tan I and Tan II treatment on vasculogenesis and angiogenesis.

Won et al.[23] found that Tan IIA-induced apoptosis involves mitochondria intrinsic caspase activation cascade and an inhibition of the PI3K/AKT survival pathway in prostate cancer cells. Therefore, we propose that Tan IIA might act *via* suppression of the VEGF/VEGFR signal pathway in tumor cells, indirectly inhibiting downstream PI3K/AKT signaling pathway, up-regulating the expression of apoptosis-promoting gene, down-regulating the expression of anti-apoptosis gene, thereby inhibiting the growth of tumor cells and promoting apoptosis.

The PI3K/AKT signal path is an important function in cell growth, migration, invasion and apoptosis, which has multiple activation mechanisms, including VEGF. The combination of VEGF and the receptor VEGFR2 can activate PI3K/AKT/Forkhead signal pathways in endothelial cells, and consequently inhibit cell apoptosis, promote DNA production and accelerate the transformation of cell cycle from the G1 stage to the S stage[24].

Collectively, Tan IIA may be an inhibitor of the VEGF/VEGFR2. It regulates MMP-2/-9 secretion and stimulates the relative cyclin and apoptin. Tan IIA also indirectly inhibits downstream the PI3K/AKT signal pathway, and overall contributes to the anti-angiogenic activity, cell proliferation inhibition, and pro-apoptosis effects. Although the mechanisms of Tan IIA's effects on the NSCLC cell line, and the genes relevant to VEGF and VEGFR2 remain to be fully explored, this is a promising direction for further research.

It is notable that Yang and others[25] found that Tan IIA could up-regulate the expression of VEGF and SDF-1 in rats' bone marrow-derived endothelial progenitor cells (EPCs), probably

promoting EPCs homing better in ischemic conditions and facilitating the effective repair of vessels.

Therefore, we propose that Tan IIA may protect normal cells, but inhibit cancer cells. However, further validation of this hypothesis is required.

In the final stages of this work, we simulated the mode of interaction between Tan IIA and targeted proteins by the virtual docking research platform. The methods were optimized by use of the results of molecular biological experiments. We focused on the analysis of the possible binding mode of Tan IIA and VEGFR2. The inhibitor actions which target the VEGF/VEGFR pathway are divided into 2 categories at present: (1) combining with VEGF to block its interaction with the receptor. For example, antibody soluble receptors and nucleic acid drugs respectively combine with VEGF in protein and nucleic acid level to inhibit angiogenesis. (2) Targeting VEGFR directly, such as antibody and inhibitors of tyrosine kinase receptor[26]. As Tan IIA is a small molecule compound, the strategy of our experiment is to target the tyrosine kinase region of VEGFR2 directly.

In PDB database, the three-dimensional structure of 3VHE, whose resolution ratio is 1.55Å, consists of a peptide chain that includes 359 amino acid residues. It contains VEGFR2 protein kinase structural domain, in which there is a new pyrrole pyrimidine derivatives inhibitor[27]. The RMSD is 0.35Å after docking again with endogenous ligand by CDOCKER module in DS2.1. Site1, the binding site we found by DS2.1 automatically searching, can cover the structural domain included by endogenous ligand. We found, after molecule docking in two ways, Tan IIA docking with the binding site of endogenous ligand is more stable. The active site of the docking of Tan IIA and VEGFR2 (PDB ID: 3VHE) may be defined as the structural domain of the binding site of endogenous ligand, according to related references[28]. This domain, whose radius is 9.5Å, contains the kinase domain of VEGFR2. Tan IIA can stably dock with the kinase structural domain of the binding site of endogenous ligand (Fig. 7D). In this kinase structural domain, two amino acid residues, Val848 and Cys917, involve with the interaction between Tan IIA and VEGFR2. The 10 configurations of Tan IIA can form hydrogen bond with Cys917 and π–π interaction with Val848 (Fig. 7D). Considering the present experiments along with the results of Won and others[23], we suggest that Tan IIA may, *via* inhibition of the VEGF/VEGFR signal pathway, inhibit the downstream PI3K/AKT signal pathway indirectly, up-regulate the expression of apoptosis-promoting genes, down-regulate the expression of anti-apoptosis genes, thereby inhibiting the growth and promoting tumor cell apoptosis. Therefore, there is strong support for the hypothesis that Tan IIA is a tyrosine kinase inhibitor of VEGFR2.

In summary, our study revealed that the mechanism of Tan IIA's anti-tumor effects may be related to inhibition of tumor angiogenesis, as a tyrosine kinase inhibitor of VEGFR2 (Fig. 8). It might interdict VEGF/VEGFR signal pathways, leading to cell cycle arrest and suppressing downstream signal pathway indirectly, then up-regulating the expression of apoptosis-promoting genes, down-regulating the expression of anti-apoptosis genes, and finally inhibiting the growth and promoting the apoptosis of tumor cells.

Based on our findings, we propose that Tan IIA could have considerable therapeutic effects in inhibiting tumor growth, angiogenesis and metastasis. In conclusion, the presence of Tan IIA may be a promising alternative therapy for NSCLC. This study otherwise suggests a new research approach to examine the active agents in traditional Chinese medicine in inhibiting tumor growth.

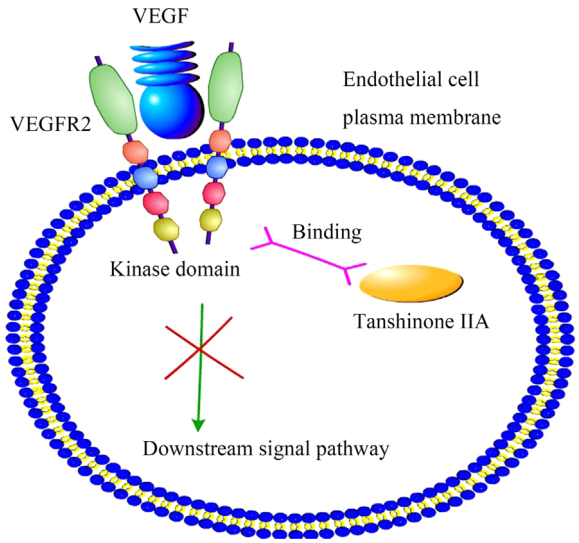

Figure 8 Molecular mechanisms of effect of tanshinone IIA in the VEGF/VEGFR signaling pathway. In vascular endothelial cells, after the VEGF combined with VEGFR2, tanshinone IIA binds to the VEGFR2 kinase domain, blocking the downstream pathways of VEGF/VEGFR.

Acknowledgment

This study was supported by the National Natural Science Foundation of China (No. 81274135).

References

1. Ferlay J, Soerjomataram I, Dikshit R, Eser S, Mathers C, Rebelo M, et al. Cancer incidence and mortality worldwide: sources, methods and major patterns in GLOBOCAN 2012. *Int J Cancer* 2015;**136**:E359–86.
2. Ettinger DS, Akerley W, Bepler G, Blum MG, Chang A, Cheney RT, et al. Non-small cell lung cancer. *J Natl Compr Canc Netw* 2010;**8**:740–801.
3. Siegel R, Ma J, Zou Z, Jemal A. Cancer statistics, 2014. *CA Cancer J Clin* 2014;**64**:9–29.
4. Hanušová V, Boušová I, Skálová L. Possibilities to increase the effectiveness of doxorubicin in cancer cells killing. *Drug Metab Rev* 2011;**43**:540–57.
5. Sharif MR, Shaabani A, Mahmoudi H, Nikoueinejad H, Akbari H, Einollahi B. Association of the serum vascular endothelial growth factor levels with benign prostate hyperplasia and prostate malignancies. *Nephrourol Mon* 2014;**6**:e14778.
6. Kaplan RN, Riba RD, Zacharoulis S, Bramley AH, Vincent L, Costa C, et al. VEGFR1-positive haematopoietic bone marrow progenitors initiate the pre-metastatic niche. *Nature* 2005;**438**:820–7.
7. di Costanzo F, Mazzoni F, Micol Mela M, Antonuzzo L, Checcacci D, Saggese M, et al. Bevacizumab in non-small cell lung cancer. *Drugs* 2008;**68**:737–46.
8. Zhou C, Wu YL, Chen G, Liu X, Zhu Y, Lu S, et al. Beyond: a randomized, double-blind, placebo-controlled, multicenter, phase III study of first-line carboplatin/paclitaxel plus bevacizumab or placebo in Chinese patients with advanced or recurrent nonsquamous non-small-cell lung cancer. *J Clin Oncol* 2015;**33**:2197–204.
9. Fu Y, Hu J, Du N, Jiao S, Li F, Li X, et al. Bevacizumab plus chemotherapy *versus* chemotherapy alone for preventing brain metastasis derived from advanced lung cancer. *J Chemother* 2015 Jun 3. Available from: http://dx.doi.org/10.1179/1973947815Y.0000000045.

10. Liu S, Kurzrock R. Toxicity of targeted therapy: implications for response and impact of genetic polymorphisms. *Cancer Treat Rev* 2014;**40**:883–91.
11. Sung HJ, Choi SM, Yoon Y, An KS. Tanshinone IIA, an ingredient of *Salvia miltiorrhiza* BUNGE, induces apoptosis in human leukemia cell lines through the activation of caspase-3. *Exp Mol Med* 1999;**31**:174–8.
12. Chen Y, Zhu J, Zhang W. Antitumor effect of traditional Chinese herbal medicines against lung cancer. *Anticancer Drug* 2014;**25**:983–91.
13. Zhai XM, He SX, Ren MD, Chen JH, Wang ZL, Han M, et al. Effect of tanshinone II A on expression of EGF and EGFR in hepatocellular carcinoma cell line SMMC-7721. *J Zhejiang Univ (Med Sci)* 2009;**38**:163–9.
14. Jing J, Zheng H, WANG J, Lin P, Zhang J, Xiong ZJ, et al. Growth inhibition and multidrug resistance-reversing effect of tanshinone IA on human breast cancer cell with estrogen receptor negative. *J Sichuan Univ (Med Sci Ed)* 2007;**38**:391–5.
15. Xing Y, Tu J, Zheng L, Guo L, Xi T. Anti-angiogenic effect of tanshinone IIA involves inhibition of the VEGF/VEGFR2 pathway in vascular endothelial cells. *Oncol Rep* 2015;**33**:163–70.
16. Tung YT, Chen HL, Lee CY, Chou YC, Lee PY, Tsai HC, et al. Active component of Danshen (*Salvia miltiorrhiza* Bunge), tanshinone I, attenuates lung tumorigenesis *via* inhibitions of VEGF, cyclin A, and cyclin B expressions. *Evid Based Complement Alternat Med* 2013;**2013**:319247.
17. Cheng CY, Su CC. Tanshinone IIA may inhibit the growth of small cell lung cancer H146 cells by up-regulating the Bax/Bcl-2 ratio and decreasing mitochondrial membrane potential. *Mol Med Rep* 2010;**3**:645–50.
18. Chiu TL, Su CC. Tanshinone IIA induces apoptosis in human lung cancer A549 cells through the induction of reactive oxygen species and decreasing the mitochondrial membrane potential. *Int J Mol Med* 2010;**25**:231–6.
19. Zhang J, Wang J, Jiang JY, Liu SD, Fu K, Liu HY. Tanshinone IIA induces cytochrome c-mediated caspase cascade apoptosis in A549 human lung cancer cells *via* the JNK pathway. *Int J Oncol* 2014;**45**:683–90.
20. Wei X, Zhou L, Hu L, Huang Y. Tanshinone IIA arrests cell cycle and induces apoptosis in 786-O human renal cell carcinoma cells. *Oncol Lett* 2012;**3**:1144–8.
21. Ma ZL, Zhang BJ, Wang DT, Li X, Wei JL, Zhao BT, et al. Tanshinones suppress AURKA through up-regulation of miR-32 expression in non-small cell lung cancer. *Oncotarget* 2015;**6**:20111–20.
22. Shibuya M. VEGF–VEGFR signals in health and disease. *Biomol Ther* 2014;**22**:1–9.
23. Won SH, Lee HJ, Jeong SJ, Lee HJ, Lee EO, Jung DB, et al. Tanshinone IIA induces mitochondria dependent apoptosis in prostate cancer cells in association with an inhibition of phosphoinositide 3-kinase/AKT pathway. *Biol Pharm Bull* 2010;**33**:1828–34.
24. Abid MR, Guo S, Minami T, Spokes KC, Ueki K, Skurk C, et al. Vascular endothelial growth factor activates PI3K/Akt/forkhead signaling in endothelial cells. *Arterioscler Thromb Vasc Biol* 2004;**24**:294–300.
25. Yang Y, Chen QW, Cao GY, Li GQ. Efficiency of rat bone marrow-derived endothelial progenitor cells on VEGF and SDF-1 expression with the aid of tanshinone IIA. *Laser J* 2012;**33**:83–6.
26. Takahashi S. Vascular endothelial growth factor (VEGF), VEGF receptors and their inhibitors for antiangiogenic tumor therapy. *Biol Pharm Bull* 2011;**34**:1785–8.
27. Oguro Y, Cary DR, Miyamoto N, Tawada M, Iwata H, Miki H, et al. Design, synthesis, and evaluation of novel VEGFR2 kinase inhibitors: discovery of [1,2,4]triazolo[1,5-*a*]pyridine derivatives with slow dissociation kinetics. *Bioorg Med Chem* 2013;**21**:4714–29.
28. Wang Z, Wang N, Han S, Wang D, Mo S, Yu L, et al. Dietary compound isoliquiritigenin inhibits breast cancer neoangiogenesis *via* VEGF/VEGFR-2 signaling pathway. *PLoS One* 2013;**8**:e68566.